CHALMERS | UNIVERSITY OF GOTHENBURG

PREPRINT 2012:7

Combined Discrete-Ordinates and Streamline Diffusion for a Flow Described by BGK Model

M. ASADZADEH
E. KAZEMI
R. MOKHTARI

Department of Mathematical Sciences
Division of Mathematics
CHALMERS UNIVERSITY OF TECHNOLOGY
UNIVERSITY OF GOTHENBURG
Gothenburg Sweden 2012

Preprint 2012:7

Combined Discrete-Ordinates and Streamline Diffusion for a Flow Described by BGK Model

M. Asadzadeh, E. Kazemi, and R. Mokhtari

Department of Mathematical Sciences
Division of Mathematics
Chalmers University of Technology and University of Gothenburg
SE-412 96 Gothenburg, Sweden
Gothenburg, May 2012

Preprint 2012:7
ISSN 1652-9715

Matematiska vetenskaper
Göteborg 2012

COMBINED DISCRETE-ORDINATES AND STREAMLINE DIFFUSION FOR A FLOW DESCRIBED BY BGK MODEL

M. ASADZADEH [1,†], E. KAZEMI[1,2], AND R. MOKHTARI[2]

Abstract. A rarefied gas flow through a channel with arbitrary cross section is studied based on the BGK model. The discrete velocity and streamline diffusion finite element methods are combined to yield a numerical scheme. For this method we derive stability and optimal error estimates in the L_2 norm. The optimality is due to the maximal available regularity of the exact solution for the corresponding hyperbolic pde. The potential of the proposed method is illustrated through implementing some numerical examples.

1. Introduction

In this paper we study the approximate solution for the flow of gas through a channel with arbitrary cross section, described by the linearized two-dimensional Bhatnagar-Gross-Krook (BGK) kinetic equation [4] using a discrete velocity model, in the discrete ordinates (DO) setting approximating in velocity, combined with the streamline diffusion (SD) finite element discretization in the spatial variable.

The physical problem has diverse applications in, e.g. micro-electromechanical systems and nanotechnology. Microducts, microturbines or vacuum equipments are the examples of small industrial devices involving the gas flow at an arbitrary Knudsen number. Since numerical solution of the Boltzmann equation in general geometry requires a six dimensional phase space grid (three dimensions in each physical and velocity domains), the computational effort in full dimensions is seemingly involved. Nevertheless, in certain physical systems due to flow conditions, certain linearizations of the governing kinetic equation and reducing the number of space and velocity coordinates can be applicable. Therefore, in general, constructing effective numerical methods for this type of multi-dimensional problems sought for physically relevant assumptions, that might circumvent computational challenges. In this regard, and in the realm of the discrete ordinates, the discrete velocity model has been developed as one of the most common techniques for the numerical solution of the, space homogeneous, Boltzmann equation and related kinetic models [6, 7]. This method has been successfully applied to solve mixture problems [9] and also some more general models including polyatomic gases with chemical reactions [5]. The discrete velocity scheme is based on replacing the collision integral term by a certain quadrature sum and requires that the resulting, dicretized, equations are valid only at discrete velocities corresponding to the numerical integration nodes. Then, the scheme is further discretized in the spatial variable by, e.g. a consistent finite difference method. Additional difficulties arise for the domains with curved boundaries in space. To deal with such geometries it is more adequate to employ some versions of the finite element method. In this regard, e.g. the streamline diffusion (SD) finite element method is a generalized

1991 *Mathematics Subject Classification.* 65M15, 65M60, 76P05.

Key words and phrases. rarefied gas, linearized BGK model, discrete velocity streamline diffusion, stability, convergence.

† Partially supported by the *Swedish Foundation of Strategic Research (SSF) in Gothenburg Mathematical Modeling Center (GMMC)* and Swedish Research Council (VR).

form of the standard Galrekin method for the hyperbolic problems having both good stability and high accuracy properties. The SD-method, used for our purpose in this paper, is obtained by modifying the test function through adding a multiple (roughly, of the order of the mesh parameter) of the convective term involved in the equation. This gives a weighted least square control of the residual of the finite element solution. For a detailed description of the SD method we refer to the monograph by Hughes and Brooks [13], and papers [14], [15], and the references therein.

An outline of this paper is as follows. Section 2 contains notation and preliminaries, where we also introduce our continuous kinetic model and describe some notation used throughout the paper. Section 3 is devoted to construction of some discrete velocity models as reasonable weak approximations for the Boltzmann collision operator. We also propose a scheme for spatial discretization based on the SD approach. Finally, we present some results concerning steady kinetic problems. In our concluding Section 4, we justify the theory through implementing some numerical examples.

2. Notations and preliminaries

Under certain physical constrains, the distribution of gas molecules may be described by the Boltzmann equation. Due to the number of unknown variables and hyperbolic structure of the equation the numerical solution of this equation is rather involved, one way out is to simplify the collision operators applying a kinetic model as the one governed by the BGK equation that maintains main properties of the original equation. Such a model for a steady flow reads as: find f such that

$$\boldsymbol{v} \cdot \nabla f(\boldsymbol{v}, \boldsymbol{x}) = J(f), \tag{2.1}$$

where $\boldsymbol{x} = (x, y, z)$ is the spatial variable and $\boldsymbol{v} = (v_x, v_y, v_z)$ is the velocity vector. Further

$$J(f) = \nu \left(f^M - f \right), \tag{2.2}$$

and the gradient is taken with respect to $\boldsymbol{x}$. The collision frequency ν may depend on $\boldsymbol{x}$, and f^M is the local Maxwellian distribution with the same density, velocity and temperature as a gas having the distribution function f. The nonlinearity of the collision term is exhibited by the fact that the density, velocity and temperature parameters are functions of f. The BGK model possesses all the collisional invariants. Let the functions $\gamma_i,\ i = 0, \ldots, 4$ be the collision invariants with $\gamma_0 = 1$, $(\gamma_1, \gamma_2, \gamma_3) = \boldsymbol{v}$ and $\gamma_4 = |\boldsymbol{v}|^2 = |\gamma_1|^2 + |\gamma_2|^2 + |\gamma_3|^2$. To derive the linearized BGK equation, we consider f to be defined as

$$f = f_0(1 + \varepsilon g), \tag{2.3}$$

where f_0 is the absolute Maxwellian distribution, which by an appropriate choice of Galilean frame and mass and velocity units, can be assumed to be of the form

$$f_0 = \frac{1}{\pi^{3/2}} e^{-|\boldsymbol{v}|^2}, \tag{2.4}$$

and g is a certain function described below. Substituting (2.3) into (2.1), we obtain

$$\boldsymbol{v} \cdot \nabla g = \nu \left[\sum_{i=0}^{4} \gamma_i (\gamma_i, g)_{f_0} - g \right], \tag{2.5}$$

where the collision invariants $\gamma_i,\ i = 0, \cdots, 4$ are normalized by the scalar product

$$(f, g)_{f_0} = \int f(\boldsymbol{v}) g(\boldsymbol{v}) d f_0. \tag{2.6}$$

It can be easily seen that the collision operator defined by

$$\mathcal{C}(g) = \left[\sum_{i=0}^{4} \gamma_i(\gamma_i, g)_{f_0} - g\right], \tag{2.7}$$

is symmetric with respect to the inner product (2.6) and satisfies $(\mathcal{C}(g), g)_{f_0} \leq 0$. Further we have

$$\text{Ker } \mathcal{C} = \left\{\sum_{i=0}^{4} c_i\gamma_i : c_i \in \mathbb{R}\right\}. \tag{2.8}$$

The Poiseuille flow, i.e. the flow of a gas through a long channel having a restricted width induced by a density, temperature or pressure gradient, likewise the Couette flow, i.e. the flow of a gas between parallel plates induced by moving them with opposite velocities; can be modeled by the linearized BGK equation. In the case of Poiseuille flow, we may represent the function g in (2.3) by

$$g(x, y, z, \boldsymbol{v}) = z + \psi(x, y, \boldsymbol{v}), \tag{2.9}$$

and obtain the following equation for ψ,

$$v_x\frac{\partial\psi}{\partial x} + v_y\frac{\partial\psi}{\partial y} = \delta(2v_z u - \psi(x, y, \boldsymbol{v})) - v_z, \tag{2.10}$$

where we used the typical assumption in fluid dynamics for long pipes that the velocity normal to wall is zero. Here δ is a rarefaction parameter and

$$u(x, y) = \frac{1}{\pi^{\frac{3}{2}}}\int v_z e^{-|\boldsymbol{v}|^2}\psi(x, y, \boldsymbol{v})d\boldsymbol{v}. \tag{2.11}$$

Multiplying equation (2.10) by $\frac{v_z}{\sqrt{\pi}}e^{-v_z^2}$ and integrating with respect to v_z we obtain

$$v_x\frac{\partial\phi}{\partial x} + v_y\frac{\partial\phi}{\partial y} = \delta(u - \phi(x, y, v_x, v_y)) - \frac{1}{2}, \tag{2.12}$$

where

$$\phi(x, y, v_x, v_y) = \frac{1}{\sqrt{\pi}}\int v_z e^{-v_z^2}\phi\, dv_z, \tag{2.13}$$

and u, corresponding to (2.11) with two-dimensional velocity, is the bulk velocity defined by

$$u(x, y) = \frac{1}{\pi}\int\int e^{-v_x^2-v_y^2}\phi(x, y, v_x, v_y)dv_x dv_y. \tag{2.14}$$

Hence, we consider the following two-dimensional integro-differential equation

$$\boldsymbol{v}\cdot\nabla f(\boldsymbol{v}, \boldsymbol{x}) = \delta\mathcal{C}(f) + S(\boldsymbol{v}, \boldsymbol{x}), \tag{2.15}$$

with boundary condition

$$f(\boldsymbol{v}, \boldsymbol{x}) = 0, \qquad \boldsymbol{x} \in \Gamma_{\boldsymbol{v}}^-, \tag{2.16}$$

where

$$\mathcal{C}(f) = \frac{1}{\pi}\int f(\boldsymbol{v}, \boldsymbol{x})e^{-|\boldsymbol{v}|^2}d\boldsymbol{v} - f(\boldsymbol{v}, \boldsymbol{x}), \tag{2.17}$$

and for each $\boldsymbol{v} \in \mathbb{R}^2$,

$$\Gamma_{\boldsymbol{v}}^- = \{\boldsymbol{x} \in \partial\Omega : \mathbf{n}\cdot\boldsymbol{v} < 0\}. \tag{2.18}$$

Here, $\boldsymbol{x} = (x, y)$, $\boldsymbol{v} = (v_x, v_y)$, Ω is the spatial domain and $\mathbf{n}$ is the outward unit normal to $\partial\Omega$ at the point $\boldsymbol{x} \in \partial\Omega$. As we mentioned earlier the two-component vectors $\boldsymbol{x}$ and $\boldsymbol{v}$, are defined in the cross section sheet of the channel. $S(\boldsymbol{v}, \boldsymbol{x})$ is an arbitrary source term and as it is shown, e.g. for recovery of the Poiseuille flow in the channel, that the source term is $S(\boldsymbol{v}, \boldsymbol{x}) \equiv -\frac{1}{2}$. Finally δ, known as the rarefaction parameter, is an important dimensionless flow quantity which characterizes the

rarefaction degree of gas. The boundary condition represents particles departing from the wall. To proceed, we introduce the scalar product

$$(f,g)_\rho = \int fg d\rho(\boldsymbol{v}), \tag{2.19}$$

where $d\rho(\boldsymbol{v}) = \frac{1}{\pi}e^{-|v|^2}$. Then, the collision operator $\mathcal{C}$ is symmetric with respect to this inner product. Moreover, Ker $\mathcal{C}$ is nontrivial and $\mathcal{C}$ is strictly negative on the orthogonal complement of the vector $\gamma_0 = 1$ (i.e. orthogonal to the space of constants). A quantity of practical interest, used later on, is the dimensionless flow rate

$$G = \frac{2}{|\Omega|}\int_\Omega u(\boldsymbol{x})d\boldsymbol{x}, \tag{2.20}$$

with $|\Omega|$ being the area of the cross section and $u(\boldsymbol{x})$ is the bulk velocity for (2.15), defined by

$$u(\boldsymbol{x}) = \frac{1}{\pi}\int f(\boldsymbol{v},\boldsymbol{x})e^{-|v|^2}d\boldsymbol{v}. \tag{2.21}$$

We set

$$\langle f,g\rangle_{\Gamma_v^\pm} = \int_{\Gamma_v^\pm} fg(\boldsymbol{v}\cdot\mathbf{n})ds, \tag{2.22}$$

where

$$\Gamma_{\boldsymbol{v}}^\pm = \{\boldsymbol{x}\in\Gamma := \partial\Omega : \boldsymbol{v}\cdot\mathbf{n} \gtrless 0\}. \tag{2.23}$$

Throughout the paper C will denote a constant not necessarily the same at each occurrence and independent of all involved parameters and functions, unless otherwise specifically specified. By $(.\,,.)_Q$ we denote the usual $L_2(Q)$ scalar product and by $\|.\|_Q$ the corresponding $L_2(Q)$-norm. Finally, we use the standard notation for Sobolev spaces together with their norms and seminorms (cf. [1]).

3. Discrete ordinates and Streamline diffusion method

In order to define discrete-ordinates/SD method for the problem (2.15)-(2.18), we first approximate the integration term appearing in the collision operator (2.17) using certain quadrature rule. To this end, we write the numerical quadrature to be used in the form

$$\int_{\mathbb{R}^2} F(\boldsymbol{v})d\sigma \sim \sum_{\boldsymbol{v}\in\Delta}\omega_{\boldsymbol{v}}F(\boldsymbol{v}), \tag{3.1}$$

where $\omega_{\boldsymbol{v}}$ are positive weights such that $\sum_{\boldsymbol{v}\in\Delta}\omega_{\boldsymbol{v}} \equiv 1$, and Δ is a discrete set of nodes defined below. Using the polar coordinate $\boldsymbol{v} = (c\cos\theta, c\sin\theta)$ with $c = |\boldsymbol{v}|$ in the quadrature rule above, we have that

$$\int_0^{2\pi}\int_0^\infty F(c,\theta)e^{-c^2}c\,dc\,d\theta \sim \sum_{\boldsymbol{v}\in\Delta}\omega_{\boldsymbol{v}}F(\boldsymbol{v}). \tag{3.2}$$

Let now

$$\Delta = \{\boldsymbol{v}_{ij} :\ \boldsymbol{v}_{ij} = c_i(\cos(\theta_j),\sin(\theta_j)),\ 1\le i\le N,\ 1\le j\le M\}, \tag{3.3}$$

be the quadrature set, with the uniform angular discretization $\theta_j = 2\pi j/M$, and the radial quadrature points $c_i = r_i/\sqrt{2}$ where r_i are the zeros of Hermite orthogonal polynomials on $(0,\infty)$ associated with the distribution $d\sigma(r) = \frac{1}{2\pi}re^{-\frac{1}{2}r^2}dr$. The number of quadrature points in Δ is then $n = MN$. Our error analysis for the discrete-ordinates (DO)/ SD method works for general quadrature rule for (2.21). For a quadrature rule of the form (3.1), which is exact for polynomials of degree $\le m$, one can prove that, see [2],

$$\left|\int_{\mathbb{R}^2} F(\boldsymbol{v})d\sigma - \sum_{\boldsymbol{v}\in\Delta}\omega_{\boldsymbol{v}}F(\boldsymbol{v})\right| \le Cm^{-\alpha}\|F\|_\alpha, \qquad \forall\, F\in H^\alpha(\mathbb{R}^2),\quad \alpha\ge 1. \tag{3.4}$$

Note that α, the maximal available regularity of F, can by non-integer. Then the collision operator $\mathcal{C}$ in (2.17) can be approximated by the discretized operator $\hat{\mathcal{C}}$ given by

$$\hat{\mathcal{C}}(f) = -f(c,\theta,\boldsymbol{x}) + \sum_{i=1}^{N}\sum_{j=1}^{M}\omega_{ij} f(c_i,\theta_j,\boldsymbol{x}). \tag{3.5}$$

Using the quadrature rule (3.5), we can discretize (2.15) in the velocity space to get

$$\begin{cases} \boldsymbol{v}_{ij}.\nabla f^{ij} = \delta\hat{\mathcal{C}}(f^{ij}) + S^{ij}, & \text{in} \quad \Delta\times\Omega, \\ f^{ij} = 0 & \text{on} \quad \Gamma^{-}_{ij}. \end{cases} \tag{3.6}$$

Here, f^{ij} is an approximation of $f(\boldsymbol{v}_{ij},\cdot)$ and $\Gamma^{-}_{ij} =: \Gamma^{-}_{\boldsymbol{v}_{ij}}$ is the inflow boundary with $\boldsymbol{v}_{ij}$ defined in (3.3). The equation system (3.6) is a first-order hyperbolic problem in the spatial domain, which will be further discretized by the SD method. We write $\boldsymbol{g} := \{g^{ij}\}_{i,j}$ or simply $\boldsymbol{g} := \{g^{ij}\}$ and define the subspace W by

$$W = \{\boldsymbol{g} :\ g^{ij}(\boldsymbol{x}) \in L^2(\Omega), \quad \boldsymbol{v}_{ij}\cdot\nabla g^{ij}(\boldsymbol{x}) \in L^2(\Omega), \ \text{ with } \ g^{ij}\,|_{\Gamma^{-}_{ij}} = 0\}. \tag{3.7}$$

For $\boldsymbol{f},\boldsymbol{g}\in W$, we define the scalar product

$$\langle\langle \boldsymbol{f},\boldsymbol{g}\rangle\rangle = \sum_{i=1}^{N}\sum_{j=1}^{M}\omega_{ij}\int_{\Omega} f^{ij}g^{ij}d\boldsymbol{x}. \tag{3.8}$$

Recalling the definition of the operator $\hat{\mathcal{C}}$, we find that for any two distribution functions $\boldsymbol{f}$ and $\boldsymbol{g}\in W$,

$$\langle\langle \hat{\mathcal{C}}(\boldsymbol{f}),\boldsymbol{g}\rangle\rangle = \langle\langle \boldsymbol{f},\hat{\mathcal{C}}(\boldsymbol{g})\rangle\rangle. \tag{3.9}$$

Now, by the Cauchy-Schwarz inequality and the fact that $\sum_{i,j}\omega_{ij}\le 1$, we find that

$$\begin{aligned} \langle\langle \hat{\mathcal{C}}(\boldsymbol{f}),\boldsymbol{f}\rangle\rangle &= \sum_{i,j}\omega_{ij}\int_{\Omega}\hat{\mathcal{C}}(f^{ij})f^{ij}d\boldsymbol{x} \\ &= \int_{\Omega}\Big(-\sum_{i,j}\omega_{ij}(f^{ij})^2 + \sum_{i,j}\omega_{ij}f^{ij}\sum_{i,j}\omega_{ij}f^{ij}\Big)d\boldsymbol{x} \le 0. \end{aligned} \tag{3.10}$$

The relation (3.10) may be referred as the non-positivity property of the discrete collision operator. It is seen from (3.9) and (3.10) that the discrete collision operator $\hat{\mathcal{C}}$ is symmetric, non-positive and, by applying the Cauchy-Schwarz inequality, bounded in the space W with inner product $\langle\langle .,.\rangle\rangle$, i.e. for all $\boldsymbol{f},\boldsymbol{g}\in W$ we have

$$-\langle\langle \hat{\mathcal{C}}(\boldsymbol{f}),\boldsymbol{g}\rangle\rangle \le 2\langle\langle \hat{\Pi}\boldsymbol{f},\hat{\Pi}\boldsymbol{f}\rangle\rangle^{1/2}\langle\langle \boldsymbol{g},\boldsymbol{g}\rangle\rangle^{1/2}. \tag{3.11}$$

Here, $\hat{\Pi}$ is the orthogonal projection onto the complement of the kernel of the discrete collision operator $\hat{\mathcal{C}}$. In order to apply the finite element method, we need to write a weak formulation for (3.6). To construct our SD finite element method, we shall use a variational formulation with a test functions consisting of the sum of a trial function g and an extra streaming term of the form $\gamma(\boldsymbol{v}\cdot\nabla g)$, i.e. we employ different test and trial function spaces. Then, for the equation (3.6), we define continuous variational formulation as: Find $\{f^{ij}\}\in W$ such that for all $\{g^{ij}\}\in W$,

$$\begin{aligned} &(\boldsymbol{v}_{ij}\cdot\nabla f^{ij}, g^{ij}+\gamma_{ij}(\boldsymbol{v}_{ij}\cdot\nabla g^{ij}))_{\Omega} - \delta(\hat{\mathcal{C}}(f^{ij}), g^{ij}+\gamma_{ij}(\boldsymbol{v}_{ij}\cdot\nabla g^{ij}))_{\Omega} \\ &\qquad = (S^{ij}, g^{ij}+\gamma_{ij}(\boldsymbol{v}_{ij}\cdot\nabla g^{ij}))_{\Omega}, \end{aligned} \tag{3.12}$$

where γ_{ij} is a positive parameter of the order of the mesh size. Multiplying by quadrature weights and summing over the quadrature set, the semi-discrete method,

for the velocity discretization, (3.12) can be written as

$$\sum_{i,j}\omega_{ij}\Big\{(\boldsymbol{v}_{ij}\cdot\nabla f^{ij},g^{ij}+\gamma_{ij}(\boldsymbol{v}_{ij}\cdot\nabla g^{ij}))_\Omega-\delta(\hat{\mathcal{C}}(f^{ij}),g^{ij}+\gamma_{ij}(\boldsymbol{v}_{ij}\cdot\nabla g^{ij}))_\Omega\Big\}$$
$$=\sum_{i,j}\omega_{ij}(S^{ij},g^{ij}+\gamma_{ij}(\boldsymbol{v}_{ij}\cdot\nabla g^{ij}))_\Omega. \tag{3.13}$$

For the spatial discretization we let $\mathcal{C}_h=\{K\}$ be a finite element subdivisions of Ω into the elements K with the mesh parameter $h=\operatorname{diam} K$. Further, let $P_k(K)$ be the set of polynomials of degree at most k on K in $\boldsymbol{x}$ and define the finite element space, viz,

$$V_h=\{g: g\in P_k(K);\ \forall K\in\mathcal{C}_h\}. \tag{3.14}$$

We also define, the finite element space associated to the semi-discrete scheme by

$$\boldsymbol{V}_h=\{\{g^{ij}\}\in(V_h)^{NM}: g^{ij}\mid_{\Gamma_{ij}^-}=0\}, \tag{3.15}$$

and introduce the corresponding bilinear form as

$$B(\boldsymbol{f}_h,\boldsymbol{g})=\sum_{i,j}\omega_{ij}\Big\{(\boldsymbol{v}_{ij}\cdot\nabla f_h^{ij},g^{ij}+\gamma_{ij}(\boldsymbol{v}_{ij}\cdot\nabla g^{ij}))_\Omega$$
$$-\delta(\hat{\mathcal{C}}(f_h^{ij}),g^{ij}+\gamma_{ij}(\boldsymbol{v}_{ij}\cdot\nabla g^{ij}))_\Omega\Big\} \tag{3.16}$$

for all $\boldsymbol{f}_h,\boldsymbol{g}\in\boldsymbol{V}_h$. Now our objective is to solve the following fully discrete variational problem: find $\boldsymbol{f}_h\in\boldsymbol{V}_h$ such that

$$B(\boldsymbol{f}_h,\boldsymbol{g})=L(\boldsymbol{g}),\qquad\forall\boldsymbol{g}\in\boldsymbol{V}_h, \tag{3.17}$$

where L is a linear form defined by

$$L(\boldsymbol{g})=\sum_{i,j}\omega_{ij}(S^{ij},g^{ij}+\gamma_{ij}(\boldsymbol{v}_{ij}\cdot\nabla g^{ij}))_\Omega. \tag{3.18}$$

For the method (3.17), we derive stability estimates and error bounds in the following norm $|||.|||$ over $\boldsymbol{V}_h$,

$$|||\boldsymbol{g}|||^2=\sum_{i,j}\omega_{ij}\Big(\gamma_{ij}\parallel\boldsymbol{v}_{ij}\cdot\nabla g^{ij}\parallel_\Omega^2+\delta\|\hat{\Pi}g^{ij}\|_\Omega^2+\int_{\Gamma_{ij}{}^+}(g^{ij})^2(\boldsymbol{v}_{ij}\cdot\mathbf{n})ds\Big), \tag{3.19}$$

where $\hat{\Pi}$ is the orthogonal projection onto the complement of the kernel of collision operator in $\boldsymbol{V}_h$. Since the space $\boldsymbol{V}_h$ is finite dimensional, we may use a Lax-Milgram approach and show that there exists a positive constant $\hat{\lambda}_0$ such that

$$\hat{\lambda}_0\langle\langle\hat{\Pi}\boldsymbol{f},\hat{\Pi}\boldsymbol{f}\rangle\rangle\le-\langle\langle\hat{\mathcal{C}}(\boldsymbol{f}),\boldsymbol{f}\rangle\rangle. \tag{3.20}$$

Below we shall show that the bilinear form B is coercive:

Lemma 3.1. *Assume that the SD parameter γ_{ij} satisfies*

$$\gamma_{ij}\sim\frac{\hat{\lambda}_0}{\delta}, \tag{3.21}$$

then, there exists a constant $\alpha>0$, depending on $\hat{\lambda}_0$, such that

$$B(\boldsymbol{g},\boldsymbol{g})\ge\alpha|||\boldsymbol{g}|||^2,\qquad\forall\boldsymbol{g}\in\boldsymbol{V}_h. \tag{3.22}$$

Proof. We let $\boldsymbol{f}^h = \boldsymbol{g}$ in (3.16), then

$$B(\boldsymbol{g},\boldsymbol{g}) = \sum_{i,j}\omega_{ij}\Big\{(\boldsymbol{v}_{ij}\cdot\nabla g^{ij}, g^{ij}+\gamma_{ij}(\boldsymbol{v}_{ij}\cdot\nabla g^{ij}))_\Omega \\ - \delta(\hat{\mathcal{C}}(g^{ij}), g^{ij}+\gamma_{ij}(\boldsymbol{v}_{ij}\cdot\nabla g^{ij}))_\Omega\Big\}. \tag{3.23}$$

Using Green's formula and the zero inflow boundary condition we get

$$(\boldsymbol{v}_{ij}\cdot\nabla g^{ij}, g^{ij})_\Omega = \frac{1}{2}\int_{\Gamma^+_{ij}}(g^{ij})^2(\boldsymbol{v}_{ij}\cdot\mathbf{n})d\boldsymbol{v}. \tag{3.24}$$

Further, by (3.20) we have

$$-\sum_{i,j}\omega_{ij}(\hat{\mathcal{C}}(g^{ij}), g^{ij})_\Omega \geq \hat{\lambda}_0\sum_{i,j}\omega_{ij}\|\hat{\Pi}g^{ij}\|^2_\Omega, \tag{3.25}$$

and using (3.11) and the Cauchy-Schwarz inequality yields

$$\sum_{i,j}\omega_{ij}\Big(\hat{\mathcal{C}}(g^{ij}), \gamma_{ij}(\boldsymbol{v}_{ij}\cdot\nabla g^{ij})\Big)_\Omega \leq 2\Big(\sum_{i,j}\omega_{ij}\|\hat{\Pi}g^{ij}\|^2_\Omega\Big)^{\frac{1}{2}}\Big(\sum_{i,j}\omega_{ij}\gamma_{ij}\|\boldsymbol{v}_{ij}\cdot\nabla g^{ij}\|^2_\Omega\Big)^{\frac{1}{2}}. \tag{3.26}$$

Hence, we deduce that

$$\sum_{i,j}\omega_{ij}\delta(\hat{\mathcal{C}}(g^{ij}), \gamma_{ij}(\boldsymbol{v}_{ij}\cdot\nabla g^{ij}))_\Omega \leq \sum_{i,j}\omega_{ij}(\hat{\lambda}_0\delta\|\hat{\Pi}g^{ij}\|^2_\Omega + \frac{\delta\gamma^2_{ij}}{\hat{\lambda}_0}\|\boldsymbol{v}_{ij}\cdot\nabla g^{ij}\|^2_\Omega), \tag{3.27}$$

Choosing γ_{ij} as in (3.21), the relations (3.23)-(3.27) yield the desired result. □

In the sequel, we shall use the following interpolation error estimates, see Ciarlet [10]: let $f \in H^{r+1}(\Omega)$ then there exists an interpolant, $\tilde{f}_h \in V_h$, of f such that

$$\|f-\tilde{f}_h\|_\Omega \leq Ch^{r+1}\|f\|_{r+1,\Omega}, \tag{3.28}$$

$$\|f-\tilde{f}_h\|_{1,\Omega} \leq Ch^{r}\|f\|_{r+1,\Omega}, \tag{3.29}$$

$$\|f-\tilde{f}_h\|_{\partial\Omega} \leq Ch^{r+1/2}\|f\|_{r+1,\Omega}. \tag{3.30}$$

Let $\{\eta^{ij}\} = \{f^{ij}\} - \{\tilde{f}^{ij}_h\}$ be the interpolation error and set $\{\xi^{ij}\} = \boldsymbol{f}_h - \{\tilde{f}^{ij}_h\}$. We may write the error as

$$\{e^{ij}\} = \{f^{ij}\} - \boldsymbol{f}_h = \{\eta^{ij}\} - \{\xi^{ij}\}. \tag{3.31}$$

The convergence theorem is now as follows:

Theorem 3.1. *Let $\{f^{ij}\}$ and $\boldsymbol{f}_h$ be the solutions of the continuous and discrete problem satisfying* (3.12) *and* (3.17)*, respectively. If the SD parameter γ_{ij} satisfies*

$$\gamma_{ij} \sim \min\Big\{\frac{\hat{\lambda}_0}{\delta}, \frac{h}{\|\boldsymbol{v}_{ij}\|_\infty}\Big\}, \tag{3.32}$$

then, there is a constant $C = C(\Omega)$ such that

$$|||\{f^{ij}\} - \boldsymbol{f}_h||| \leq Ch^{k+1/2}\Big(\sum_{i,j}\omega_{ij}(\delta+\|\boldsymbol{v}_{ij}\|_\infty)\|f^{ij}\|^2_{k+1,\Omega}\Big)^{1/2}. \tag{3.33}$$

Proof. Using the triangle inequality we have

$$|||\{e^{ij}\}||| \leq |||\{\eta^{ij}\}||| + |||\{\xi^{ij}\}|||. \tag{3.34}$$

The definition of the triple norm $|||.|||$ and the interpolation error estimates (3.28)-(3.30) yield

$$|||\{\eta^{ij}\}||| \leq Ch^{k+1/2}\Big(\sum_{i,j}\omega_{ij}(\delta+\|\boldsymbol{v}_{ij}\|_\infty)\|f^{ij}\|^2_{k+1,\Omega}\Big)^{1/2}. \tag{3.35}$$

Using the Galerkin orthogonality relation $B(\{e^{ij}\},\{\xi^{ij}\})=0$, since γ_{ij} in (3.32) fulfills (3.21), we have that

$$\begin{aligned}|||\{\xi^{ij}\}|||^2 \le B(\{\xi^{ij}\},\{\xi^{ij}\}) &= B(\{\eta^{ij}\}-\{e^{ij}\},\{\xi^{ij}\}) = B(\{\eta^{ij}\},\{\xi^{ij}\})\\ &= \sum_{i,j}\omega_{ij}\Big\{(\boldsymbol{v}_{ij}\cdot\nabla\eta^{ij},\xi^{ij}+\gamma_{ij}(\boldsymbol{v}_{ij}\cdot\nabla\xi^{ij}))_\Omega\\ &\qquad -\delta(\hat{\mathcal{C}}(\eta^{ij}),\xi^{ij}+\gamma_{ij}(\boldsymbol{v}_{ij}\cdot\nabla\xi^{ij}))_\Omega\Big\}.\end{aligned} \tag{3.36}$$

Integrating by parts and applying Cauchy-Schwarz inequality we obtain

$$\begin{aligned}(\boldsymbol{v}_{ij}\cdot\nabla\eta^{ij},\xi^{ij})_\Omega &= -(\eta^{ij},\boldsymbol{v}_{ij}.\nabla\xi^{ij})_\Omega+\frac{1}{2}\int_{\Gamma^+_{ij}}\eta^{ij}\xi^{ij}(\boldsymbol{v}_{ij}\cdot\mathbf{n})\,ds\\ &\le \gamma_{ij}^{-1}\|\eta^{ij}\|^2_\Omega+\frac{\gamma_{ij}}{4}\|\boldsymbol{v}_{ij}.\nabla\xi^{ij}\|^2_\Omega\\ &\quad+\int_{\Gamma^+_{ij}}|\eta^{ij}|^2(\boldsymbol{v}_{ij}\cdot\mathbf{n})\,ds+\frac{1}{8}\int_{\Gamma^+_{ij}}|\xi^{ij}|^2(\boldsymbol{v}_{ij}\cdot\mathbf{n})\,ds.\end{aligned} \tag{3.37}$$

Similarly to bound the second term in (3.36), we have using (3.11), the Cauchy-Schwarz inequality and (3.9) that

$$-\sum_{i,j}\omega_{ij}\delta\Big(\hat{\mathcal{C}}(\eta^{ij}),\xi^{ij}\Big)_\Omega\le\sum_{i,j}\omega_{ij}\left\{C\delta\|\eta^{ij}\|^2_\Omega+\frac{\delta}{4}\|\hat{\Pi}\xi^{ij}\|^2_\Omega\right\}, \tag{3.38}$$

and

$$-\sum_{i,j}\omega_{ij}\delta\Big(\hat{\mathcal{C}}(\eta^{ij}),\gamma_{ij}(\boldsymbol{v}_{ij}\cdot\nabla\xi^{ij})\Big)_\Omega\le\sum_{i,j}\omega_{ij}\left\{C\delta\|\hat{\Pi}\eta^{ij}\|^2_\Omega+\frac{\gamma_{ij}^2\delta}{4\hat{\lambda}_0}\|\boldsymbol{v}_{ij}\cdot\nabla\xi^{ij}\|^2_\Omega\right\}. \tag{3.39}$$

Combining the estimates (3.36)-(3.39) and using (3.32), we obtain

$$\begin{aligned}|||\{\xi^{ij}\}|||^2\le B(\eta,\xi)\le\frac{1}{4}|||\{\xi^{ij}\}|||^2+C\sum_{i,j}\omega_{ij}\Big[\gamma_{ij}^{-1}\|\eta^{ij}\|^2_\Omega+\gamma_{ij}\|\boldsymbol{v}_{ij}\cdot\nabla\eta^{ij}\|^2_\Omega\\ +\int_{\Gamma^+_{ij}}|\eta^{ij}|^2(\boldsymbol{v}_{ij}\cdot\mathbf{n})\,ds\Big].\end{aligned} \tag{3.40}$$

Using (3.28)-(3.30), a kick-back argument and (3.32) we deduce that

$$|||\{\xi^{ij}\}|||\le Ch^{k+1/2}\Big(\sum_{i,j}\omega_{ij}(\delta+\|\boldsymbol{v}_{ij}\|_\infty)\|f^{ij}\|^2_{k+1,\Omega}\Big)^{1/2}. \tag{3.41}$$

Inserting the inequalities (3.35) and (3.41) into (3.34) we obtain the desired result. □

To proceed, we decompose the global error as

$$\{f_h^{ij}\}-\{f(\boldsymbol{v}_{ij},.)\}=\{f_h^{ij}\}-\{f^{ij}\}+\{f^{ij}\}-\{f(\boldsymbol{v}_{ij},.)\}. \tag{3.42}$$

Then by triangle inequality,

$$|||\{f_h^{ij}\}-\{f(\boldsymbol{v}_{ij},.)\}|||\le|||\{f_h^{ij}\}-\{f^{ij}\}|||+|||\{f^{ij}\}-\{f(\boldsymbol{v}_{ij},.)\}|||. \tag{3.43}$$

We now bound the term $|||\{f^{ij}\}-\{f(\boldsymbol{v}_{ij},.)\}|||$ which is related to quadrature formula (3.1). To this end, we consider(2.15) for $\boldsymbol{v}=\boldsymbol{v}_{ij}$ and subtract the result from (3.6), to obtain

$$\boldsymbol{v}_{ij}\cdot\nabla\chi^{ij}-\delta\hat{\mathcal{C}}(\chi^{ij})=\rho(\boldsymbol{x}),\qquad\chi^{ij}=0\text{ on }\Gamma^-_{ij}, \tag{3.44}$$

where $\chi^{ij} = f^{ij} - f(\boldsymbol{v}_{ij}, .)$ and

$$\rho(\boldsymbol{x}) = \frac{1}{\pi}\int f(\boldsymbol{v},\boldsymbol{x})e^{-|\boldsymbol{v}|^2}d\boldsymbol{v} - \sum_{i,j}\omega_{ij}f(\boldsymbol{v}_{ij},\boldsymbol{x}). \tag{3.45}$$

Using the scalar product introduced in (2.6), and multiplying the equation (3.44) by $\{\gamma_{ij}(\boldsymbol{v}_{ij}\cdot\nabla\chi^{ij})\}$, we get that

$$\begin{aligned}\langle\langle\{\boldsymbol{v}_{ij}\cdot\nabla\chi^{ij}\},\{\gamma_{ij}(\boldsymbol{v}_{ij}\cdot\nabla\chi^{ij})\}\rangle\rangle - \delta\langle\langle\{\hat{\mathcal{C}}(\chi^{ij})\},\{\gamma_{ij}(\boldsymbol{v}_{ij}\cdot\nabla\chi^{ij})\}\rangle\rangle \\ = \langle\langle\rho,\{\gamma_{ij}(\boldsymbol{v}_{ij}\cdot\nabla\chi^{ij})\}\rangle\rangle.\end{aligned} \tag{3.46}$$

Now using the Cauchy-Schwarz inequality, (3.11) and (3.32) we end up with

$$\sum_{i,j}\omega_{ij}\gamma_{ij}\|\boldsymbol{v}_{ij}\cdot\nabla\chi^{ij}\|_\Omega^2 \le C\Big(\|\rho(x)\|_\Omega^2 + \delta^2\sum_{i,j}\omega_{ij}\|\hat{\Pi}\chi^{ij}\|_\Omega^2\Big). \tag{3.47}$$

Similarly, taking the inner product of equation (3.44) with $\{\chi^{ij}\}$, applying the Green's theorem and using the boundary condition in (3.44) we obtain

$$\frac{1}{2}\sum_{i,j}\omega_{ij}\int_{\Gamma_{ij}^+}(\chi^{ij})^2\boldsymbol{v}_{ij}\cdot\mathbf{n}\,ds - \sum_{i,j}\omega_{ij}\delta\int_\Omega\hat{\mathcal{C}}(\chi^{ij})\chi^{ij}d\boldsymbol{x} = \sum_{i,j}\omega_{ij}\int_\Omega\chi^{ij}\rho d\boldsymbol{x}. \tag{3.48}$$

Using the Cauchy-Schwarz inequality and the inequality (3.20) we deduce that

$$\frac{1}{2}\sum_{i,j}\omega_{ij}\int_{\Gamma_{ij}^+}(\chi^{ij})^2\boldsymbol{v}_{ij}\cdot\mathbf{n}\,ds + \delta\sum_{i,j}\omega_{ij}\|\hat{\Pi}\chi^{ij}\|_\Omega^2 \le CZ\|\rho\|_\Omega, \tag{3.49}$$

where $Z = \max_{i,j}\|\chi^{ij}\|_\Omega$. Now, it remains to bound the term $\|\rho\|_\Omega$. To this end, we apply the quadrature error (3.4) to ρ and to get

$$|\rho(\boldsymbol{x})| \le Cm^{-\alpha}\|f(.,\boldsymbol{x})\|_\alpha. \tag{3.50}$$

Square integration over Ω yields

$$\|\rho\|_\Omega^2 \le Cm^{-2\alpha}\int_\Omega\|f(.,\boldsymbol{x})\|_\alpha^2 d\boldsymbol{x}. \tag{3.51}$$

Finally, combining the estimates (3.47), (3.49) and (3.51) we get

$$\begin{aligned}|||\{f^{ij}\} - \{f(\boldsymbol{v}_{ij},\boldsymbol{x})\}|||^2 \le & Cm^{-2\alpha}\int_\Omega\|f(.,\boldsymbol{x})\|_\alpha^2 d\boldsymbol{x} \\ & + C\delta Zm^{-\alpha}\Big(\int_\Omega\|f(.,\boldsymbol{x})\|_\alpha^2 d\boldsymbol{x}\Big)^{1/2}.\end{aligned} \tag{3.52}$$

Now we formulate the main result of this paper:

Theorem 3.2. *Let f be the exact solution satisfying the equations* (2.15)-(2.18). *Assume that $f \in H^\alpha(\mathbb{R}^2, H^{k+1}(\Omega))$ and the quadrature approximation* (3.4) *is valid. Then, there is a constant $C > 0$, independent of h and m, such that for the fully discrete problem* (3.17)-(3.18) *the following estimate holds true*

$$\begin{aligned}|||\{f_h^{ij}(\boldsymbol{x})\} - \{f(\boldsymbol{v}_{ij},\boldsymbol{x})\}|||^2 \le & Ch^{2k+1}\sum_{i,j}\omega_{ij}(\delta + \|\boldsymbol{v}_{ij}\|_\infty)\|f^{ij}\|_{k+1,\Omega}^2 \\ & + m^{-2\alpha}\int_\Omega\|f(.,\boldsymbol{x})\|_\alpha^2 d\boldsymbol{x} + (\delta Zm^{-\alpha})\Big(\int_\Omega\|f(.,\boldsymbol{x})\|_\alpha^2 d\boldsymbol{x}\Big)^{1/2}.\end{aligned} \tag{3.53}$$

Proof. Using the triangle inequality (3.43), Theorem 3.1 and the estimate (3.52) yield the desired result. □

Remark 3.1. Here are some features of the problem (2.15)-(2.18): lack of absorption term in equation (2.15) yields to stability with no explicit L_2-norm control. Actually we obtain the L_2-norm stability of orthogonal projection onto the complement of the kernel of the discrete collision operator. By some transformation (an exponential variable substitution), we may obtain an equation having an absorption term, then the kernel of the integral operator will be changed. We may also consider some properties of the operator $\boldsymbol{v}_{ij} \cdot \nabla$ leading to an $L_2(\Omega)$ estimate. Since $\nabla \cdot \boldsymbol{v}_{ij} = 0$, the convection operator $\boldsymbol{v}_{ij} \cdot \nabla : W \to L_2(\Omega)$ is an isomorphism (see, e.g., [11] and the references therein) and we have that

$$\alpha \|g\|_\Omega \leq \|\boldsymbol{v}_{ij} \cdot \nabla g\|_\Omega, \qquad \forall g \in W, \tag{3.54}$$

for some constant $\alpha > 0$. Note that in all the above estimates the semi-norm, (L_2-norm of partial derivatives), appears with a coefficient of order $\mathcal{O}(\sqrt{h})$. Combining this and Theorem 3.2, the coefficients γ_{ij} will appear in the L_2-norm estimates as well. Therefore, in implementations, one should expect to get an actual rate of convergence of order $\mathcal{O}(h^k + m^{-\alpha} h^{-\frac{1}{2}})$, i.e. a rate reduced by the order of $h^{1/2}$, compared to the theory. Based on this phenomena, we may remove the last term in (3.53) and improve the error estimate.

As a result of the Theorem 3.2 and Remark 3.1, we may obtain an order of convergence for the mass flow rate G introduced by (2.20).

Corollary 3.3. *Assume that G is the mass flow rate defined by* (2.20)*, and its approximation, G_h, is given by*

$$G_h = \frac{1}{|\Omega|} \sum_{i,j} \omega_{ij} \int_\Omega f_h^{ij}(\boldsymbol{x}) d\boldsymbol{x}. \tag{3.55}$$

Then we have

$$|G - G_h| \sim C_\delta^{-1} \mathcal{O}(\delta^{1/2} h^{k+1/2} + m^{-\alpha} + \delta^{1/2} m^{-\alpha/2}). \tag{3.56}$$

where $C_\delta = \min\{\delta, \frac{1}{\delta}, \gamma_{ij}\}$.

Proof. By the triangle inequality we may write

$$|G - G_h| \leq |G - \hat{G}| + |\hat{G} - G_h|, \tag{3.57}$$

where

$$\hat{G} = \frac{1}{|\Omega|} \sum_{i,j} \omega_{ij} \int_\Omega f(\boldsymbol{v}_{ij}, \boldsymbol{x}) d\boldsymbol{x}. \tag{3.58}$$

Applying the quadrature error (3.4), for the first term in (3.57) we have

$$|G - \hat{G}| \leq C m^{-\alpha} \int_\Omega \|f(., \boldsymbol{x})\|_\alpha d\boldsymbol{x}. \tag{3.59}$$

In addition, using Hölder inequality, for the second term in (3.57) we obtain

$$|\hat{G} - G_h| \leq \sum_{i,j} \omega_{ij} \|f(\boldsymbol{v}_{ij}, .) - f_h^{ij}\|_\Omega. \tag{3.60}$$

Now, by Theorem 3.2 and Remark 3.1 we deduce that

$$|\hat{G} - G_h| \sim C_\delta^{-1} \mathcal{O}(\delta^{1/2} h^{k+1/2} + m^{-\alpha} + \delta^{1/2} m^{-\alpha/2}), \tag{3.61}$$

where $C_\delta = \min\{\delta, \frac{1}{\delta}, \gamma_{ij}\}$. Then inserting (3.59) and (3.61) into (3.57), and using the regularity assumption on f, we obtain the desired result. □

4. Numerical investigations

To justify the theoretical results, in this section, we compute the mass flow rates in the wide range of rarefaction parameter δ for rectangular, triangular and circular cross sections. The results are compared with those in the literature: [16], [17], [20] and [21]. We also investigate the performance of the proposed method on numerical convergence order in the norm $|||.|||$ defined by (3.19). In the considered examples, we have used piecewise linear polynomials with the mish size $h = 0.07$. We have also used the quadrature formula with $M = 15$ and $N = 15$, i.e. 225 ordinates. Since $-\hat{\mathcal{C}}$ is a symmetric positive semi-definite operator, the parameter $\hat{\lambda}_0$ in (3.32) may be approximated by Rayleigh quotient and thus we have $\hat{\lambda}_0 \leq \min_{i,j}(1-\omega_{ij})$, where ω_{ij} are the weights in the quadrature formula (3.1). We choose γ_0 of the streamline-diffusion parameter: $\gamma = \gamma_0 h$ to be equals to 0.01 for $\delta \leq 5$, and 0.001 for $\delta > 5$, and subject to the constraint (3.32). Finally, for the case of $\delta < 10$ the resulting linear algebraic system of equations is solved using a successive over-relaxation solver and the stopping criterion on the convergence of the iterative procedure is set equal to 10^{-12}. Since for $\delta \gg 1$, the convergence of the iteration method slows down, we have employed direct method in solving the discretized systems. In the Table 1 we present the results of calculating the flow rate G in rectangular channels and compare these results with the corresponding data from [17] and [18] for different aspect ratios a/b, where $2a$ is the maximum tube length in the x direction and $2b$ is the maximum tube length in the y direction. In Table 2 the computed results for the circular and elliptical cross sections are presented. These results are generally in good (within 1%) agreement with the published results in [12] and [16] over the entire δ range. Some exceptions appear for the cases $\delta \gg 1$ and $\delta \ll 1$, where the difference between the results is slightly larger than 1%. This is due to the presence of δ in approximation error formula (3.53). We may use higher order quadrature rule, and finer mesh parameter in the physical domain for the cases of $\delta \ll 1$ and $\delta \gg 1$, respectively. Table 3 is for flows in triangular channels. The computed results are compared with those in [20], which are only presented for the δ-vales up to $\delta = 50$.

These results are demonstrated through some plots, where in the Figure 1 the velocity distributions in a rectangular channel are plotted for different values of the rarefaction parameter $\delta = 0.01, 0.1, 1$ and 10. In the Figures 2 and 4, the u level sets in a circular and an equilateral triangular channel are plotted for different values of γ_0 and for the rarefaction parameters $\delta = 0.1$ and $\delta = 1$, respectively. One may see the smoothing effects of the SD-parameter on corresponding Figures. In the Figure 3 we also present the velocity level sets for a right-angle triangular cross-section and for different values of δ.

We now present a numerical example for solving the boundary value problem and illustrate the performance of the proposed method on numerical convergence.

Example 4.1. In this example, we study our problem considering the spatial domain to be the unit square $[0,1] \times [0,1]$ and with the source function given by

$$\begin{aligned} S(\boldsymbol{v},\boldsymbol{x}) =& w(\theta,\boldsymbol{x}) + cw(\theta,\boldsymbol{x})\cos(\theta)\big(\theta y \sin(\pi x)\sin(\pi y) + \pi\theta xy\cos(\pi x)\sin(\pi y)\big) \\ &+ cw(\theta,\boldsymbol{x})\sin(\theta)\big(\theta x sin(\pi x) sin(\pi y) + \pi\theta xy\cos(\pi y)\sin(\pi x)\big) \\ &- (\frac{1}{2\pi}(e^{2\pi xy\sin(\pi x)\sin(\pi y)} - 1))/(xy\sin(\pi x)\sin(\pi y)), \end{aligned}$$

where

$$w(\theta,\boldsymbol{x}) = e^{\theta xy\sin(\pi x)\sin(\pi y)}. \tag{4.1}$$

This example is particularly designed, so that the exact solution is given by

$$u(\boldsymbol{v},\boldsymbol{x}) = w(\theta,\boldsymbol{x}) - 1. \tag{4.2}$$

TABLE 1. Reduced flow rate G in rectangular channels vs rarefaction parameter δ and aspect ratio a/b.

δ	G					
	a/b=1		a/b=2		a/b=10	
	[17, 18]	(3.17)	[18]	(3.17)	[18]	(3.17)
.01	0.8281	0.8201	1.137	1.1229	1.910	1.9407
.02	0.8213	0.8160	1.125	1.1145	1.858	1.8896
.05	0.8076	0.8055	1.099	1.0944	1.759	1.7880
.1	0.7934	0.7925	1.073	1.0716	1.665	1.6876
.2	0.7766	0.7765	1.046	1.0462	1.563	1.5785
.5	0.7622	0.7603	1.026	1.0243	1.454	1.4568
.8	0.7614	0.7609	1.031	1.0288	1.425	1.4246
1	0.7678	0.7652	1.041	1.0377	1.424	1.4213
1.5	0.7861	0.7827	1.074	1.0700	1.448	1.4419
2	0.8076	0.8056	1.115	1.1100	1.491	1.4834
5	0.9885	0.9787	1.413	1.3977	1.870	1.8633
10	1.329	1.3161	1.955	1.9559	2.599	2.5981
15	1.705	1.6591	2.511	2.5166	3.357	3.3636
20	2.000	2.0066	3.077	3.0831	4.121	4.1405
30		2.7071		4.2219		5.7088
40		3.4102		5.3616		7.2861
50		4.1136		6.4991		8.8677
100		7.6136		12.1268		16.7988
200		14.4824		23.0328		32.6890

TABLE 2. Reduced flow rate G in elliptical channels vs rarefaction parameter δ and aspect ratio a/b.

δ	G							
	a/b=1		a/b=1.1		a/b=2		a/b=10	
	[16]	(3.17)	[12]	(3.17)	[12]	(3.17)	[12]	(3.17)
.01	1.4760	1.4650	1.548	1.5360	2.066	2.0025	3.314	3.3414
.02	1.4598	1.4538	1.529	1.5237	2.015	1.9802	3.198	3.2208
.05	1.4295	1.4280	1.497	1.4958	1.985	1.9335	2.994	3.0048
.1	1.4026	1.4018	1.469	1.4680	1.935	1.8912	2.817	2.8169
.2	1.3816	1.3790	1.446	1.4447	1.893	1.8587	2.651	2.6427
.5	1.3864	1.3835	1.499	1.4525	1.881	1.8777	2.534	2.5158
.8	1.4252	1.4214	1.499	1.4958	1.951	1.9473	2.565	2.5419
1	1.4583	1.4540	1.536	1.5323	2.009	2.0040	2.614	2.5877
1.5	1.5532	1.5477	1.641	1.6365	2.170	2.1629	2.780	2.7457
2	1.6576	1.6507	1.757	1.7505	2.344	2.3345	2.976	2.9337
5	2.3483	2.3301	2.516	2.5138	3.471	3.4677	4.331	4.3242
10	3.5633	3.5619	3.850	3.8488	5.430	5.4299	6.738	6.7717
20	6.0411	6.0453	6.565	6.5689	9.402	9.4135	11.65	9.2620
30	8.5333	8.5416	9.294	9.3015	13.39	13.4086	16.58	16.7387
40	11.0295	11.0378	12.03	12.0334	17.39	17.3983	21.52	21.6815
50	13.5269	13.5303	14.76	14.7608	21.38	21.3777	26.46	26.5811
100	26.0214	25.9028		28.2975		41.0770		50.4005
200	51.0254	50.1348		54.8049		79.4233		94.8108

TABLE 3. Reduced flow rate G in various triangular channels vs rarefaction parameter δ.

δ	G					
	equilateral		scalene		orthogonal isosceles	
	[20]	(3.17)	[20]	(3.17)	[20]	(3.17)
0.001	0.929	0.9109	0.935	0.9162	0.965	0.9464
0.01	0.919	0.9054	0.925	0.9106	0.954	0.9400
0.1	0.872	0.8692	0.878	0.8734	0.902	0.8985
0.5	0.831	0.8277	0.835	0.8303	0.854	0.8501
0.75	0.829	0.8259	0.833	0.8279	0.851	0.8465
1	0.834	0.8301	0.837	0.8317	0.854	0.8494
1.5	0.851	0.8475	0.855	0.8484	0.870	0.8651
2	0.876	0.8711	0.879	0.8716	0.894	0.8877
5	1.06	1.0581	1.07	1.0584	1.08	1.0744
10	1.41	1.4083	1.42	1.4090	1.43	1.4278
20	2.14	2.1408	2.14	2.1443	2.17	2.1709
30	2.88	2.8858	2.89	2.8929	2.92	2.9278
40	3.62	3.6350	3.63	3.6456	3.67	3.6889
50	4.37	4.3857	4.38	4.3994	4.43	4.4512
100		8.1352		8.1565		8.2501
200		15.5503		15.5442		15.7193

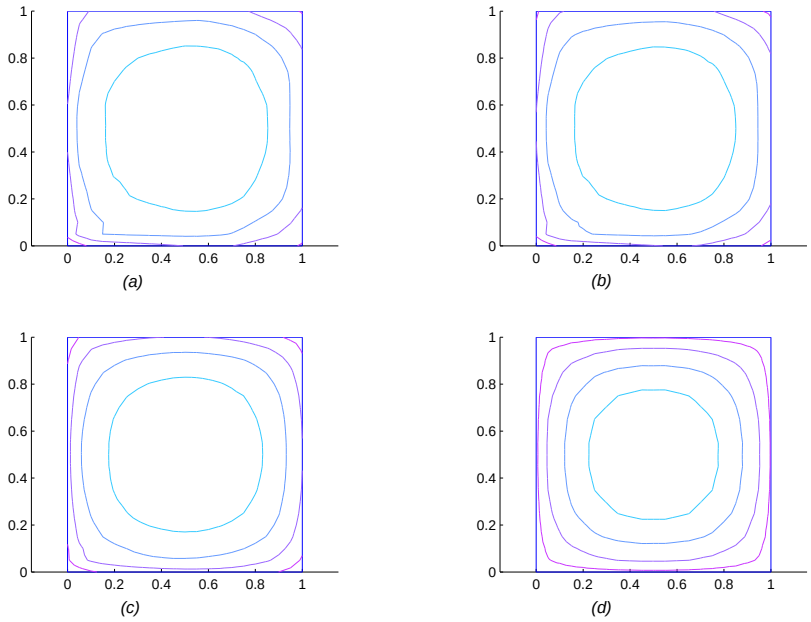

FIGURE 1. Velocity contours in the cross section of a square channel: (a-d) related to $\delta = 0.01, 0.1, 1$ and 10.

To compute the spatial errors, we will use the standard strategy considering higher order approximations in the quadrature rule (3.1) and then compute the convergence order of the space discretization. In Tables 4-5 and Figure 5, we show these convergence results in the L_2-norm, as well as the $|||.|||$-norm defined by (3.19). We

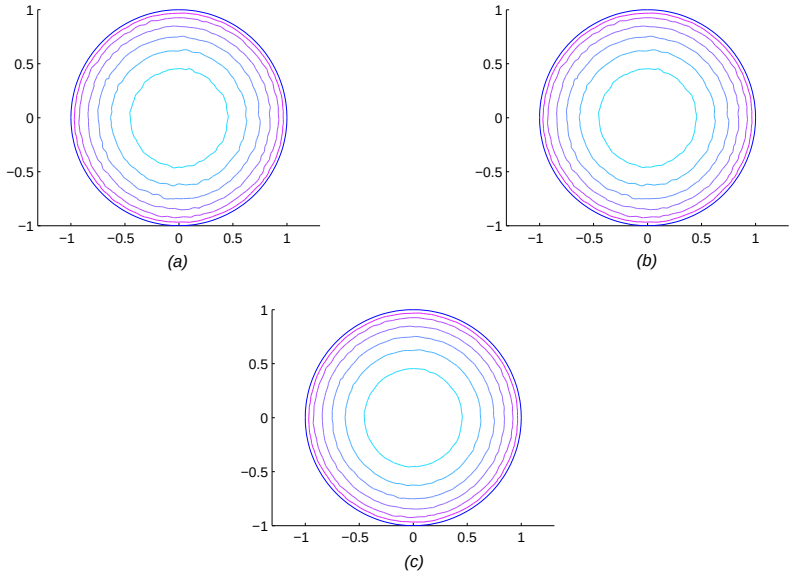

FIGURE 2. Comparison of the velocity contours for the unit circle with $\delta = 0.1$: (a-c) related to $\gamma_0 = 0, 0.001$ and 0.01.

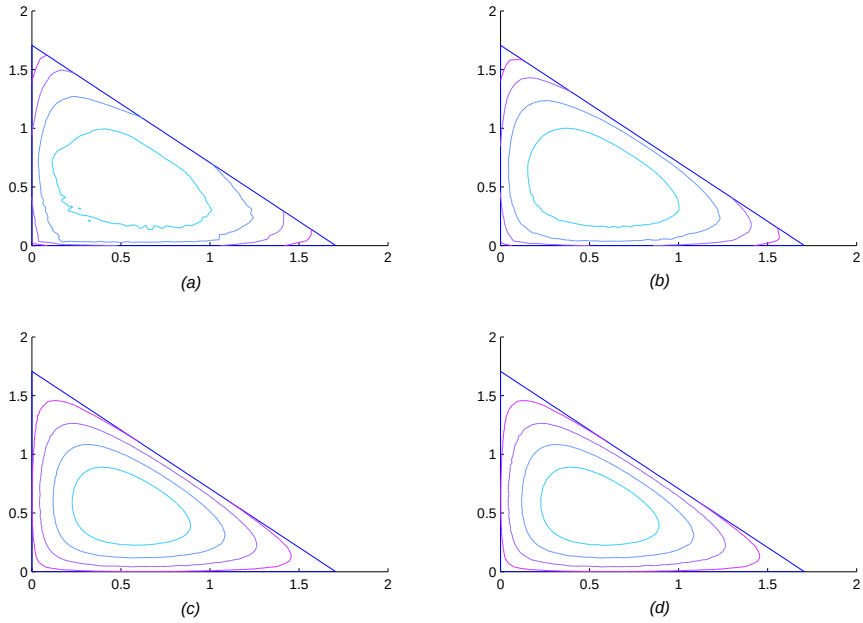

FIGURE 3. Velocity contours for the orthogonal triangle: (a-d) related to $\delta = 0.01, 0.1, 1$ and 10.

also present the error of the mass flow rate G, defined by (2.20), in Table 6 and Figure 6, for the different values of γ_0.
To see the influence of the numerical quadrature error on the solution accuracy, we also use the less refined numerical quadrature with $M = 5$ and $N = 5$, i.e. only 25 ordinates. For instance, corresponding to $h = \frac{\sqrt{2}}{20}$ the errors for the numerical

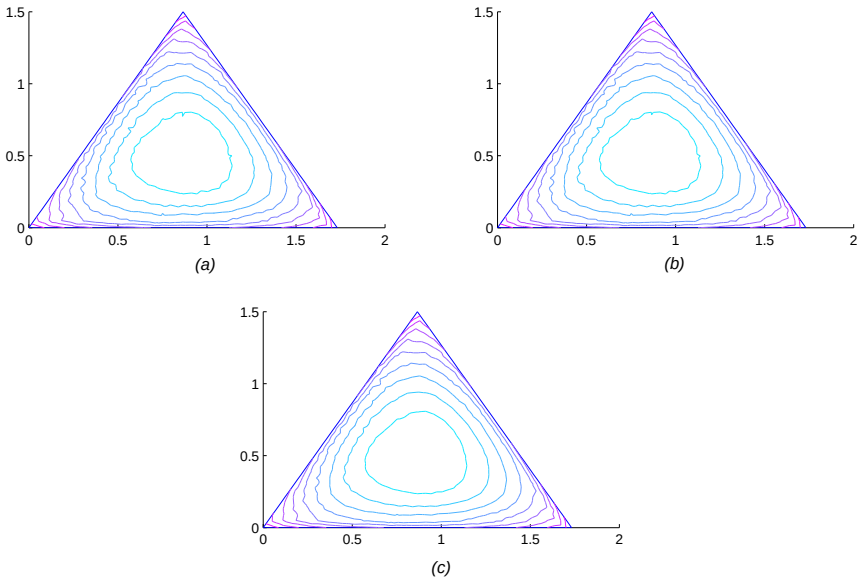

FIGURE 4. Comparison of the velocity contours for the equilateral triangle with $\delta = 1$: (a-c) related to $\gamma_0 = 0, 0.001$ and 0.01.

TABLE 4. Error $\|u - u_h\|$ for Example 4.1.

h	$\gamma_0 = 0$	$\gamma_0 = 0.001$	$\gamma_0 = 0.01$	$\gamma_0 = 0.1$	$\gamma_0 = 0.5$
$\frac{\sqrt{2}}{5}$	0.247206982	0.244798006	0.227213803	0.178063742	0.216327675
$\frac{\sqrt{2}}{10}$	0.026715009	0.02652664	0.025652036	0.030466757	0.0759276
$\frac{\sqrt{2}}{15}$	0.011670016	0.01150648	0.010821089	0.013734404	0.045281935
$\frac{\sqrt{2}}{20}$	0.006162771	0.006065313	0.005766944	0.008593496	0.032996712

TABLE 5. Error $|||u - u_h|||$ for Example 4.1.

h	$\gamma_0 = 0$	$\gamma_0 = 0.001$	$\gamma_0 = 0.01$	$\gamma_0 = 0.1$	$\gamma_0 = 0.5$
$\frac{\sqrt{2}}{5}$	0.303022935	0.304333116	0.316307008	0.420452474	0.718022365
$\frac{\sqrt{2}}{10}$	0.029895327	0.032654345	0.051285278	0.132921852	0.284534964
$\frac{\sqrt{2}}{15}$	0.013185436	0.014826665	0.025414045	0.070742315	0.16144478
$\frac{\sqrt{2}}{20}$	0.006925584	0.008218338	0.01572285	0.045652177	0.107539983

TABLE 6. Error $|G - G_h|$ for Example 4.1.

h	$\gamma_0 = 0$	$\gamma_0 = 0.001$	$\gamma_0 = 0.01$	$\gamma_0 = 0.1$	$\gamma_0 = 0.5$
$\frac{\sqrt{2}}{5}$	0.086942268	0.086250263	0.080363851	0.044469892	0.007591975
$\frac{\sqrt{2}}{10}$	0.006840345	0.006843534	0.007019878	0.007931986	0.007860636
$\frac{\sqrt{2}}{15}$	0.003764336	0.003679156	0.003300136	0.003239473	0.004556734
$\frac{\sqrt{2}}{20}$	0.001084447	0.00109074	0.001217363	0.001589597	0.002807666

solution in the L_2-norm: $\|u-u_h\|$ for the different (see the Tables 4-6) values for the parameter γ_0 are, respectively, 0.00681873, 0.006722791, 0.006416259, 0.009199408,

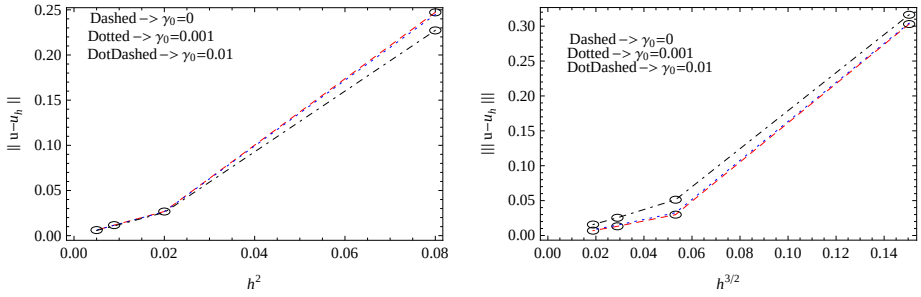

FIGURE 5. $\|u - u_h\|$ vs. h^2 (left) and $|||u - u_h|||$ vs. $h^{3/2}$ (right) for Example 4.1.

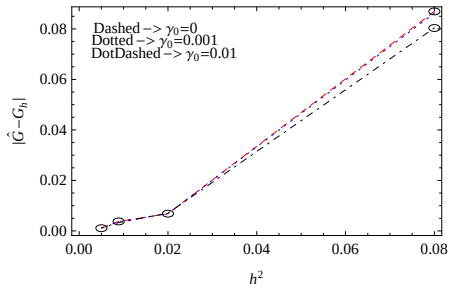

FIGURE 6. $|G - G_h|$ vs. h^2 for Example 4.1.

0.033521166 and those for $|||u - u_h|||$ are, respectively, 0.007871414, 0.007699679, 0.007173271, 0.010485591, 0.037295534. Thus the errors in the numerical solution are mainly due to the spatial discretization. We have varied γ_0 in the SD-parameter $\gamma = \gamma_0 h$ in (3.32) to check the influence of stabilization parameter on the fully discrete solution. In Table 4 we see that increasing γ_0 further, L_2 error increases due to smearing.

Conclusion. The fully developed flow of a rarefied gas in a channel with arbitrary cross section, due to an imposed pressure gradient, is described by a BGK model. This paper concerns stability and convergence of a fully discrete scheme for a linear BGK equation. The discretization is based on a discrete-ordinates method for the velocity variable combined with the streamline diffusion finite element method in the spatial domain. We derive optimal convergence rates due to the maximal available regularity of the exact solution. In the numerical investigations, results for the velocity profiles and the flow rate have been provided for various geometries for the flow channel with the rectangular, circular and triangular cross sections, in the whole range of rarefaction parameter δ. The convergence rates in both L_2- and the triple-norm, $|||\cdot|||$, are justified for a generic example in a square spatial domain.

In contrast to the previous published results, the solution herein is extended easily into the near continuum regime. In addition, it seems that the present method can be used to solve other physically relevant models derived from the Boltzmann equation.

References

[1] H. Adams, *Sobolev Spaces*, Academic Press, New York, (1978).

[2] M. Asadzadeh, *Analysis of a fully discrete scheme for neutron transport in two-dimensional geometry*, SIAM J. Numer. Anal., 23 (1986), no. 3, 543-561.

[3] M. Asadzadeh, *Streamline diffusion methods for Fermi and Fokker-Planck equations*, Transport Theory Statist. Phys. 26 (1997), no. 3, 319-340.

[4] P. L. Bhatnagar, E. P. Gross, and M. Krook, *A model for collision processes in gases*, Phys. Rev., 94 (1954), 511-515.

[5] V. Bobylev and C. Cercignani, *Discrete velocity models without nonphysical invariants*, J. Statist. Phys., 97 (1999), 677-689.

[6] A. V. Bobylev, A. Palczewski and J. Schneider, *On approximation of the Boltzmann equation by discrete velocity models*, C. R. Acad. Sci. Paris Sr. I Math., 320 (1995), no. 5, 639-644.

[7] C. Buet, *A discrete-velocity scheme for the Boltzmann operator of rarefied gas dynamics*, Transport Theory Statist. Phys., 25 (1996), no. 1, 33-60.

[8] C. Cercignani, *The Boltzmann Equation and its Applications*, Springer-Verlag, New York, 1988.

[9] C. Cecignani and A. V. Bobylev, *Discrete velocity models: The case of mixtures*, Transport Theory Statist. Phys., 29 (2000), 209-216.

[10] P. G. Ciarlet, *The Finite Element Method for Elliptic Problems*, North-Holland, Amsterdam, 1978.

[11] A. Ern and J.-L. Guermond, *Theory and Practice of Finite Elements*, Appl. Math. Sci. 159, Springer-Verlag, New York, 2004.

[12] I. Graur and F. Sharipov, *Gas flow through an elliptical tube over the whole range of the gas rarefaction*, Eur. J. Mech. B. Fluids, 27 (2008), 335-345.

[13] Hughes T. J. R., and Brooks A., *A Multidimensional Upwind Scheme With No Crosswind Diffusion*, Finite Element Methods for Convection Dominated Flows, Ed. T. J. R. Hughes, AMD Vol. 34, ASME, New York (1979).

[14] Hughes T. J. R., and Mallet M., *A New Finite Element Formulation for Computational Fluid Dynamics III, The Generalized Streamline Operator for Multidimensional Advective—Diffusive Systems*, Comput. Methods Appl. Mech. Engrg. 58 pp. 305-328 (1986).

[15] C. Johnson, J. Saranen, *Streamline diffusion methods for the incompressible Euler and Navier-Stokes equations*, Math. Comp. 47 (1986), no. 175, 1-18.

[16] S. S. Lo and S. K. Loyalka, *An efficient computation of near-continuum rarefied gas flows*, Z. Angew. Math. Phys. (ZAMP), 33 (1982), 419-424.

[17] S. K. Loyalka, T. S. Storvik and H. S. Park, *Poiseuille flow and thermal creep flow in long, rectangular channels in the molecular and transition flow regimes*, J. Vac. Sci. Technol., 13 (1976), 1188-1192.

[18] F. Sharipov, *Rarefied gas flow through a long rectangular channel*, J. Vac. Sci. Technol. A, 17 (1999), 3062-3066.

[19] D. Valougeorgis and S. Naris, *Acceleration schemes of the discrete velocity method: gaseous flows in rectangular microchannels*, SIAM J. Sci. Comput., 25 (2003), no. 2, 534-552.

[20] D. Valougeorgis and S. Naris, *Rarefied gas flow in a triangular duct based on a boundary fitted lattice*, Eur. J. Mech. B. Fluids, 27 (2008), 810-822.

[21] D. Valougeorgis and J. R. Thomas, *Exact numerical results for Poiseuille and thermal creep flow in a cylindrical tube*, Phys. Fluids., 29 (2) (1986), 423-429.

[1] Department of Mathematics, Chalmers University of Technology and Göteborg University, SE–412 96, Göteborg, Sweden

E-mail address: mohammad@chalmers.se

[2] Department of Mathematical Sciences, Isfahan University of Technology, Isfahan 84156-83111, Iran